Title: New insights into non-contact reflectance IR mapping of teeth

Authors

Franco Lizzi[1], Hamza Elfarraj[1], Oleksandra Maruschenko[1,3], Ole Lenz[1], Peter Lasch[4], Ljiljana Puskar[5], Ioanna Mantovalou[2,3], Paul Zaslansky[1].

(1) Charité – Universitätsmedizin Berlin, Aßmannshauser Straße 4-6, 14497 Berlin, Germany;

(2) Institute for Optics and Atomic Physics, Technical University of Berlin, Hardenbergstr. 36, 10623 Berlin, Germany; Berlin laboratory for innovative X-ray technologies – BLiX

(3) Helmholtz-Zentrum Berlin für Materialien und Energie, Hahn-Meitner-Platz 1, 14109 Berlin, Germany;

(4) Robert Koch-Institute (RKI), Center for Biological Threads and Special Pathogens, ZBS 6 - Proteomics and Spectroscopy, Nordufer 20, 13353, Berlin, Germany

(5) Helmholtz-Zentrum für Materialien und Energie, 12489, Berlin, Germany

Abstract

Teeth are made of highly mineralized tissues that withstand years of daily usage. Their mechanical properties have been studied at all length scales with ageing but manly small areas have been the focus of high-sensitivity chemical property quantification. A comprehensive, spatially resolved examination across centimeter sized tooth specimens is needed to expand our comprehension of young versus aged teeth. Specular Reflectance Fourier Transform Infrared Spectroscopy (srFTIR) is a nondestructive microscopy technique that can be used to characterize the chemical composition of mineralized surfaces. This technique provides spatially resolved chemical absorption information, making it useful to study both organics and mineral in visibly accessible tooth tissues. Highly polished dehydrated cross-sectional surfaces of bovine and human teeth were srFTIR imaged, and spectra were processed using a Kramers-Kronig Transformation to generate absorbance-like chemical maps. Results are comparable with the well-established FTIR Transmission and Attenuated Total Reflection (ATR) methods. Maps of multiple ν_3-phosphate vibrations, ν_2-carbonate, and amide I reveal insights into structural and chemical variations across dentine. Young bovine teeth exhibited many chemical and structural similarities to old, partially sclerotic human teeth, affirming their use as proxies in dental research. This work highlights the capability of specular reflection infrared spectroscopy imaging to reveal spatial chemical information and expand our understanding of tooth microstructure and composition variations.

Introduction

Teeth are ubiquitous biologically grown mineralized cutting-tools, made primarily of an outer layer of enamel surrounding dentine that shapes the crown and the roots while protecting a pulp chamber and living tissue in the center (Figure 1). Unlike enamel that is highly crystalline, dense and hard, dentine forms a porous bulk, with micron-sized tubules radiating outwards from the pulp, terminating in enamel in the crown and in a thin layer of external cementum in the roots [1]. The mineralized tissues of teeth comprise carbonated apatite ($Ca_{10}(PO_4)_6COH$) in different forms: long crystals in enamel and nanocrystals embedded in collagen in dentine and cementum. It is impressive that human and other teeth are able to withstand years of daily mechanical load from mastication, yet unlike rodents and other mammals that continuously grow teeth (e.g. beavers), tooth tissues are not replaced/regrown. With no tissue turnover, teeth inspire extensive investigations into their mechanical and chemical properties in relation to the microstructure [2][3]. Usually, such studies address the chemistry only in relatively confined, small areas, albeit at high resolution, thus hampering comparisons across entire tooth specimens [4][5]. This is important, because both the normal as well as ageing microstructures emerge gradually. Indeed, non-contact, non-destructive chemical mapping of large tooth sections remains a technical challenge.

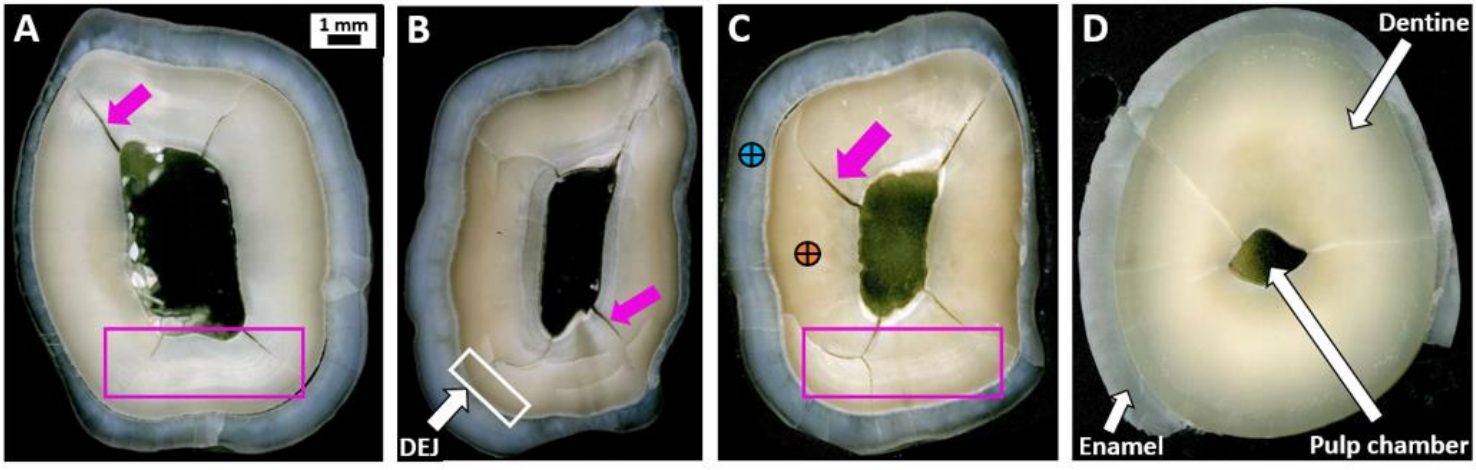

Figure 1 – Optical images at 20x of three bovine (indicated by A, B, C) and one human (D) teeth. Arrows in D indicate the main visible components of teeth: Enamel, on the outer circumference, dentine forms the inner bulk surrounding the pulp chamber in the center. The dentin-enamel junction (DEJ) is connects the two materials in the tooth crown. Purple arrows indicate some examples cracks, known to appear in the teeth, as a result of dehydration.

Fourier Transform Infrared Spectroscopy (FTIR) is a well-established and widely-used chemical characterization technique that relies on measuring different absorption interactions at various wavelengths of the infrared spectrum. Measurements yield complete spectra that serve as molecular fingerprints in which specific absorption bands correspond to characteristic molecular vibrations. This method has long been used as a reliable analytical technique for investigating the chemical composition and molecular structure of many materials including biological and mineralized tissue such as bone, cartilage and teeth [6][7].

Two different FTIR modes are widely used: (i) Transmission and (ii) Attenuated Total Reflection (ATR), both offering high precision and strong signal clarity but with different working principles: (i) Transmission spectroscopy requires that the infrared beam passes through the analyzed samples which typically requires them to be thinly sliced or powdered. On the other hand, (ii) ATR spectroscopy, relies on optical coupling of the incoming IR radiation with the sample surface to avoid air in the path so as to produce an evanescent wave [6]. ATR is thus well suited to measure the surface region of thick samples but relies on pressing the optical lens into the sample surface. The choice of (i) or (ii) IR method relies to a large extent on considerations of sample preparation. This is of particular concern in research of biological hard tissues such as teeth where the structure, microstructure and arrangement are of significance. In general, transmission samples (i) demand destructive preparation that may extensively disrupt the layout of the sample (indeed, powders are preferred). Specialized microtomes can produce micrometer-thin samples that are usually also very small and fragile, which limits the observed area to a small region. More often, samples are milled into powder, a process that gives good average signal but sacrifices the spatial distribution of the analyzed sample. The more popular technique (ii), ATR spectroscopy, requires almost no preparation since the interaction is limited to the outer microns of the sample surface. It can reach high resolution and can be used for automated analysis by laterally moving the sample and repeatedly bringing the imaging tip into contact with the analyzed surface. Both methods have limitations: studies have demonstrated that the preparation procedures induce variations in the spectra obtained, as shown for example for bone [8][9]. In particular, ATR has a complex dependence on the refractive index differences between the imaging system and the analyzed material, which can complicate comparisons with spectra obtained via the transmission method [10][11]. Additionally, ATR requires good optical contact between the imaging tip and the sample, the quality of which strongly affects the measurements, especially if the sample is sensitive to pressure [12]. Bones [13] and teeth [14][15] are examples of biological materials where the mineral experiences residual stresses due to interactions with the collagen fibers. Therefore, thin-slicing (in sections 10 μm thick or less), powdering or pressurization through a contact tip will all affect the measurements, which may be a concern when examining subtle or long-range (millimeter distance) changes such as the influence of biomaterials or ageing. For such studies, non-contact specular reflectance spectroscopy (srFTIR) may be of use. This form of FTIR, similar to optical microscopy, requires mainly that the surface be highly polished to remain in focus. srFTIR thus offers spatially resolved data, with samples prepared similar to samples used in scanning electron microscopy. One major advantage of the non-contact approach is that it readily enables mapping over large surfaces of sliced mineralized samples that preserve the microstructure [6], where the optical path is not contaminated by contact with the sample/substrate. Spectra can thus be collected without the need to powder or press the sample. Nonetheless, raw reflectance data are not trivially comparable with the other FTIR methods, as they record a convoluted mixture of light reflected at different depths of the sample surface. The Kramers-Kronig transformation (KKT) offers a way to convert srFTIR data into absorbance-like spectra that are comparable to those obtained by transmission or ATR methods [16][17][18].

Specular reflection FTIR has been applied to teeth, and its use has been reported for enamel [19][20][21][22][23] as well as for the DEJ [4] and for crown dentine [24] (Fig. 1). However, while previous studies have focused on specific areas of the tooth, there remains a need for comprehensive research that examines entire cross-sections. Assessing all regions of the tooth together would provide a more complete understanding of its structural, compositional, and functional characteristics, in particular for assessing ageing.

In this study, we compare and contrast bovine and human dental crowns using srFTIR processed spectra by a revised approach to perform Kramers-Kronig transformation on large 2D maps collected over entire tooth cross sections. This approach makes it possible to identify the main chemical signatures and their variations across the samples. Comparisons with IR data obtained using more commonly employed methods, provides a blueprint for making use of this approach and reveals characteristics of bovine teeth as reasonable models for dental research relevant for human teeth.

Materials and Methods

Sample preparation:

Tooth cross section samples

Reasonably intact bovine incisor teeth were collected from slaughtered adult cows, ~4 years old, and studied alongside one human premolar extracted for unrelated periodontal health reasons, obtained from the Charité Universitätsmedizin according to the ethical guidelines of the institute. All teeth were stored at 4°C in individual vials immersed in a solution of 0.5% Chloramine-T (Sigma-Aldrich, USA) until use. Cross sections were cut with a water-cooled wafering saw (Exact 300 CL, Norderstedt, Germany) beneath the enamel cap (across the root) to yield slices with a thickness of approximately 5 mm. In all such cross sections (Fig. 1), the empty pulp chamber is identifiable in the center, surrounded by dentine and an enamel ring in the outer circumference. The slices were embedded in Technovit 4071 (Kulzer Technik, Germany) and polished (Exact Micro Grinder 400 CS) using silicon carbide grinding papers with grits from P600 up to P4000 (Buehler CarbiMet, Germany), leading to an almost mirror finish of the surface. After polishing, the samples were dried with water-diluted ethanol concentrations, increasing from 25% to 97% (v/v). Finally, they were stored in a desiccator filled with silica gel until they were scanned. In this manner, four dehydrated slices were created, three bovine and one human, each from a different tooth.

Dentine reference pellets

Sample fragments from several bovine teeth cut at the same height were used to make FTIR compatible transmission pellets. In a first step, all cementum and enamel were removed with a high-speed diamond bur N°850 dental tool under copious irrigation with water. The remaining dentine segments were cut into small pieces with a water-cooled saw and ground into powder with a laboratory mill (KM1, Janetzki, Poland). The resulting crushed mass was incrementally filtered until reaching a final filter-paper mesh size of 40 µm (DIN4188), enhanced with the aid of a mechanical shaker used to accelerate the process. The remaining powder was dried by heating in an oven at 60°C for 24 hours. The dry powder was mixed with potassium bromide (KBr, Sigma-Aldrich, USA) to reach a ratio of 25% dentine powder to 75% KBr. The mixture was pressed (MP150, Maassen, Germany) into thin round cylinder pellets by applying 15 tons for 15 minutes. In this manner, it was possible to reach pellets of approximately 10 µm thickness.

Imaging

Optical images

A VHX-5000 digital optical microscope (Keyence, Japan) was used to capture high resolution images of the surfaces of the samples, obtained at a magnification of 20x. Images of the teeth reveal the main components: enamel, dentine and the pulp chamber. The optical images of all cross sections can be seen in the Figure 1.

Scanning Electron Microscopy (SEM)

All samples were scanned using a Phenom XL backscatter electron microscope (Thermo Fisher Scientific, Netherlands). Entire cross-sectional surface images were created by stitching together multiple high-resolution single SEM images. The scans were obtained using a magnification of 920x, a working distance of 10.3 mm, an energy of 15kV and a low vacuum of 60 Pa.

X-Ray Fluorescence (XRF)

The polished bulk samples were further mapped by micro X-ray fluorescence (µXRF). The scans were carried out using an M4 Tornado micro-XRF spectrometer (Bruker Nano GmbH, Germany) equipped with a rhodium X-ray tube. The chamber pressure was kept at 20 mbar to facilitate the detection of light elements, specifically P. The X-ray source operated at an accelerating voltage of 50 kV and a current of 1 mA. Surface mapping of the samples was conducted with a step size of 50 µm and a measurement time of 1 second per pixel. Spectral deconvolution was performed using Specfit [25], and the results were converted into 2D maps that illustrate the distribution of and concentration of the phosphorus signal.

Fourier Transform Infrared Spectroscopy (FTIR) measurements:

Specular reflection measurements

srFTIR mapping was performed with internal Globar infrared source of a Nicolet iN10 (Thermofisher, USA) at the Helmholtz-Zentrum Berlin für Materialien und Energie (HZB). An IR microscope objective of 15x magnification was used (0.7 N.A.) and a nitrogen-cooled mercury cadmium telluride (MCT) detector was used with a KBr beamsplitter, with the sample stage connected

to a dry air source to purge the instrument of humidity and CO_2 impurities. This spectrometer features a moving stage, to automatically map the whole tooth surface, with intermediate collection of background spectra obtained from a standard. For each polished slice, the area scanned included the entire cross-sectional areas of both dentine and enamel. The following parameters were used: spectral range from 700 cm^{-1} to 4000 cm^{-1}, spectral resolution of 4 cm^{-1} (no zero filling), 128 spectra per pixel, with an aperture size of 300 by 300 µm. Motors were moved with step sizes of 300 µm in both x- and y- directions in each scan. The angle of the incidence of the reflection beam is a fixed parameter of the system, set at 30°. A srFTIR spectrum of a CsI crystal was used as the background spectrum (Korth Kristalle, Germany).

Comparison with Attenuated Total Reflection (ATR) measurements

Attenuated Total Reflectance Measurements (ATR) of local areas in dentine in each sample were performed using the same spectrometer as described for the reflection measurements. Most measurement parameters were identical to those defined for the specular reflection mode with the exception of the aperture and step size, that were lowered to 100 µm to map the smaller areas at higher resolution as compared to the srFTIR measurements. A slide-on MicroTip ATR Germanium crystal was used as the measuring tip. The pressure was set arbitrarily to 15 psi, which is the minimum possible for the available machine. No noticeable damage (e.g. cracking) was detected on the sample surface after the measurement procedure.

Transmission measurements

A Vertex 70 FTIR spectrometer coupled to a Bruker Hyperion 2000 with a 15x objective and equipped with a 64×64 MCT Focal Plane Array detector (Bruker, Ettlingen, Germany) was used to measure the thin pressed 10 µm thick dentine pellets. Transmission spectra were collected in a spectral range from 350 to 8000 cm^{-1} with a spectral resolution of 4cm^{-1}. Ten scans were acquired and averaged, using a gold plate background spectrum as reference, collected at the onset of measurements.

Kramers-Kronig transformation data processing

Each of the srFTIR spectra measure in each sample was processed using in-house Python code that converts raw reflection data to IR absorbance transmission-like spectra. The code applies the Kramers-Kronig Transformation (KKT) based on the approach of Lichvar [26] and is described in the supplementary materials section, and is also freely available [27]. The transformed spectra were then imported into CytoSpec [28] and then processed by linear baseline correction near the phosphate peak at 900-1200 cm^{-1} followed by normalization to the highest peak near 1010 cm^{-1}.

Spectral correlation of srFTIR peaks

To help assess the relationship between the IR signatures and chemical and microstructural gradients across the different samples, we followed the approach of Jones et al.[29], to calculate, for different peaks in the maps, indices of "Similarity in Pattern (SIP)". This provides an estimation of the spatial covariance of the main peaks across the samples, offering some quantitative metric that can be linked to how the different absorption bands revealed in the maps, vary in space. Of particular interest were the ν_3-phosphate deconvoluted bands, as well as the amide I, and ν_2-carbonate signatures [20][30][31].The SIP was tested for a local neighborhood of 3x3 points surrounding each pixel in the maps. The constant k_1 relates to the luminance of the images and k_2 to the contrast, and were set to 0.01 and 0.03 respectively. The values chosen ensure stability in the algorithm designed by Wang et al [32].

Results and discussion:

Scanning Electron Images

All backscatter SEM images reveal both the density differences between enamel and dentin, as well as features and gradients in the microstructures, extending from enamel inward towards the pulp. Overview images and some magnified regions are shown in Figure 2. The overview images reveal the DEJ on the outer dentine margins, as well as dehydration cracks (examples marked by purple arrows) well matching the same features observed by the optical images (compare Fig. 1). At higher magnification, the characteristic µm-sized dentinal tubules become apparent. The distribution of tubules varies across dentine and can sometimes be identified by changes in the gray scale across the surface imaged by SEM. Such gradients are exemplified in magnified views marked 1, 2 and 3 in sample B, shown in the lower panel of Fig. 2

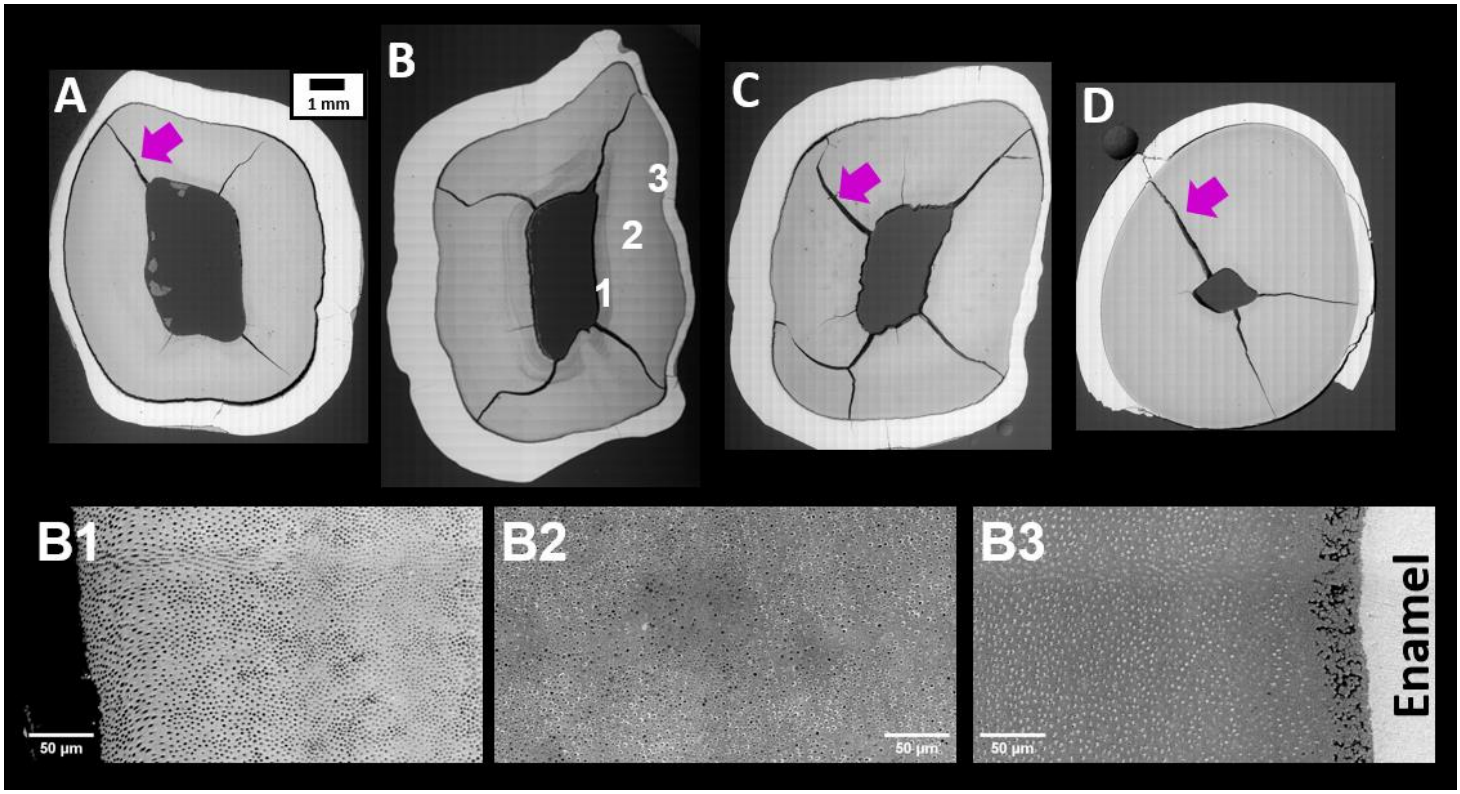

Figure 2 – Electron microscope images of the polished samples A, B, C and D. (see Fig. 1). Three example higher-magnification regions are shown for sample B, revealing gradients in the shapes and densities of dentinal tubules. In particular note that tubules appear as black hollows in B1 but attain white halos (known as peritubular dentine - PTD) in B2. Image B3 shows the DEJ region between enamel and dentine, where the tubule diameters and PTD vanish almost completely near enamel. Large voids can be seen at the interface.

In particular, near the pulp (B1), the diameter and density of tubules is higher as compared to other regions. Many tubules in the central regions of crown dentine are surrounded by a dense mineralized cuff of peritubular dentine (PTD) [33]. Towards the outer dentine junction with enamel, the tubules become smaller and less dense [34] as can be seen in B3. In some regions, dentine exhibits voids possibly interglobular dentine at the junction with enamel [35]. Importantly, the enamel is highly mineralized with apatite, which is expected to correspond to measurements by FTIR and XRF that are sensitive to the presence of phosphorus/phosphate in the mineral. Dentine, which is similar to bone, is less highly mineralized, as revealed by the lower brightness of the backscatter SEM images. Within dentine, increased presences of tubules lacking PTD will decrease the signal arising from the mineral, whereas the presence of dense PTD and in particular in combination with higher density tubules (B2) is linked to an increase in the backscatter mineral signal.

X-Ray Fluorescence (XRF)

Phosphorus intensities in the µXRF images are consistently high and uniform in the highly-crystalline enamel regions. As seen in Figure 3, the lower mineral density of dentine manifests as non-uniform gradients in the phosphorus distribution, with a near DEJ rim of lower phosphorus signal (Fig. 1, B). This corresponds to the sub-DEJ soft zone, that is less mineralized beneath enamel in human teeth [36]. Similar patterns of gradients in the phosphorus signal, with some increase observed midway between the DEJ and the pulp, appear to correlate with the distribution of dentinal tubules and in particular peritubular dentine (see Fig. 2). As the size and density of tubules decrease progressively from the pulp outward, there is initially an increase followed by a decrease in mineral content, resulting in an increase and then decrease in the phosphorus signal in those areas of all samples.

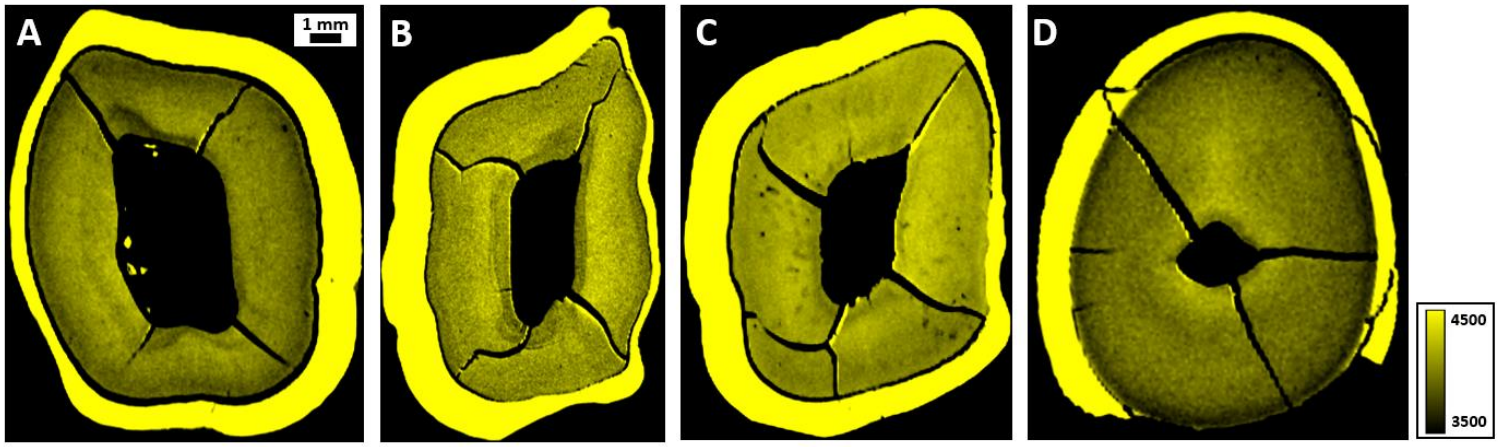

Figure 3 – Phosphorus XRF mapping of teeth A, B, C, D. The scale bar and P K-line intensity counts allow comparison between different maps. The intensity scale represents the net counts per second. Images show that enamel contains the highest signal of phosphorus, essentially a high concentration of crystalline calcium phosphates. The phosphorus distribution in dentine more or less correlates with the density of PTD and exhibits an increased density due to dentinal tubules in the circumpulpar regions of dentine, with a clear decrease in the near enamel regions (DEJ) regions, lacking PTD (Fig. 2).

Specular Reflectance IR maps

At all points measured by srFTIR, complete IR spectra were obtained. Figure 4 shows two example spectra (n=10 repeats) obtained from two spots: dentine (blue) and enamel (orange) (see Figure 1, C). The spectra reveal characteristic features of bony material known from conventional FTIR analysis methods. The enamel spectra exhibit a main peak near 1044 cm^{-1} and a second, smaller one at 1094 cm^{-1} and both were attributed in previous work to the ν_3-phosphate P-O antisymmetric stretching [20] arising in the apatite mineral. In dentine, a similar ν_3-phosphate antisymmetric stretching peak is found at 1031 cm^{-1} with a shoulder at 1090 cm^{-1}. Both dentine and enamel show a peak at 960 cm^{-1} corresponding to the ν_1-phosphate P-O stretching [20]. Other commonly reported chemical components in bone studies [37] include the ν_2 −carbonate at ~870 cm^{-1}, observed in both enamel and dentine, and the collagen protein related amide I at ~1630 cm^{-1}, which, as expected, appears only in the dentine spectra [38]. Thus, the amide I is a good representation of tooth dentine in srFTIR maps [5]. These band assignments of the prior to KKT transformation of our samples thus match with literature reports of specular reflectance FTIR reflection measurements [3][6][7].

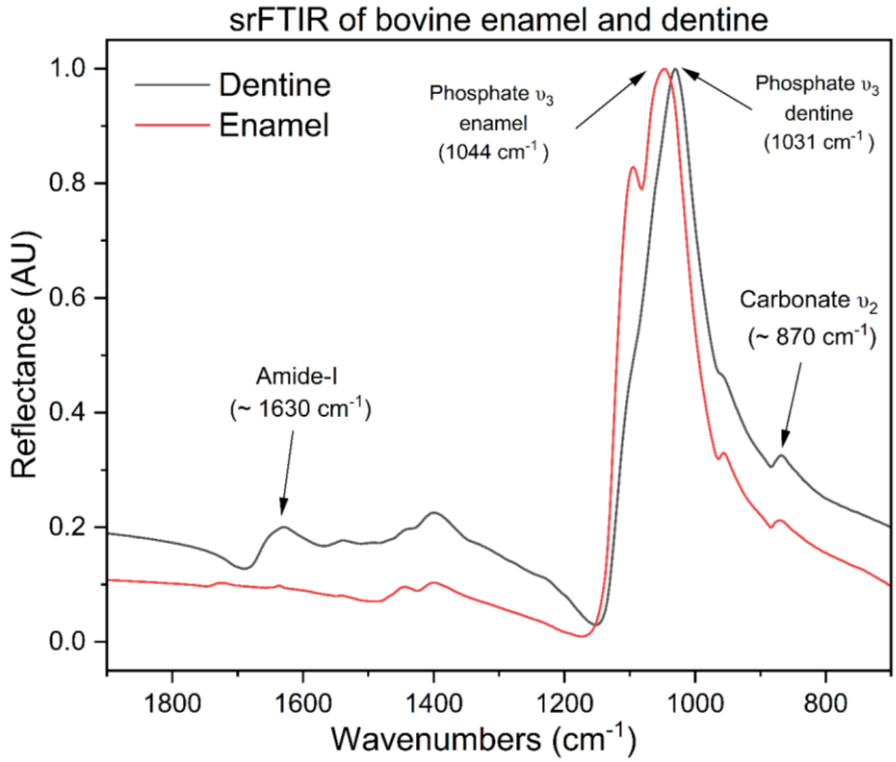

Figure 4 – Comparison of n=10 averaged srFTIR spectra collected for enamel and dentine in a highly polished bovine sample using an aperture size of 300x300µm with 128 scans per point, 4 cm^{-1} spectral resolution without zero filling. Cesium iodide was used as a background reference. The measurement points are depicted in Figure 1 sample C for enamel (orange spot) and dentine (blue spot). Several peaks can be identified in the srFTIR data in a plot of the intensity versus wavenumber. In enamel the stronger

ν_3-phosphate peak appears at wavenumber of 1044 cm^{-1} while for dentine it appears at 1031 cm^{-1}. The absorption peak of ν_2-carbonate appears at ~870 cm^{-1}In both materials. The amide I is present in dentine as is known as one of the collagen fingerprints in FTIR spectra, found at ~1630 cm^{-1}.

Conversion of srFTIR to transmission-like spectra:

Kramers Kronig transformed srFTIR (rFTIR KKT):

The specular reflection spectra were converted to absorbance-like spectra, to make the data comparable to other FTIR methods. Example spectra calculated with the Kramers-Kronig transformation code [27] provided in the supplements of this paper, show for both dentine and enamel (Fig. 5, A) a strong well-defined ν_3-phosphate band between 900 and 1200 cm^{-1}. The main peak in dentine is approximately centered at 1011 cm^{-1} whereas for enamel it appears at higher wavenumbers, 1021 cm^{-1}. The ν_1-phosphate P-O stretching band at 960 cm^{-1} is conserved for both tooth tissues. However, in dentine it appears as a separate well-defined peak while in enamel it partially overlaps with the dominant phosphate peak. The peak of ν_2-carbonate is always present at 875 cm^{-1} while amide I, the organic component at 1660 cm^{-1}, is only identifiable in dentine. A magnification of the phosphate peak and shoulders detected in the range of 900-1200 cm^{-1} is shown in Figure 5, B.

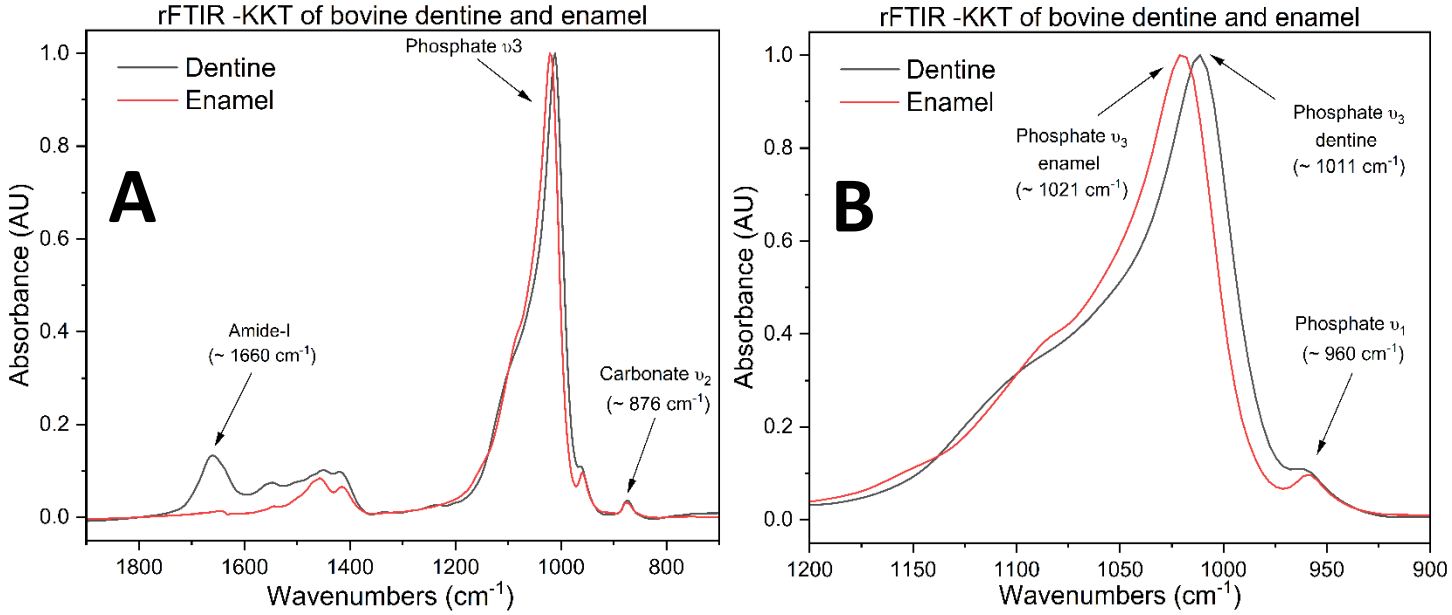

Figure 5 –A) Example Kramers-Kronig transformations of the reflection spectra from Figure 4. Band assignments of the phosphate peak as well as of the organics amide I and ν_2-carbonate shift by approximately 20 cm^{-1} as compared to the peak position in the specular reflectance measurements. The phosphate band exhibits multiple components as is also seen in transmission and ATR data. B) a magnified view of the ν_3-phosphate peak, located between 900 and 1200 cm^{-1}.

Understanding srFTIR and the relationship to tooth microstructures

The main chemical component in teeth is mineral: carbonated apatite, found in both dentine and enamel[37][38]. In dentin, the nanometer-sized tablet-shaped crystals form a composite with collagen. This protein gives rise to the major amide vibration bands observed in the wavenumber range of 1400-1700 cm^{-1} [39]. Unlike backscatter SEM that is mainly sensitive to the density and higher atomic weight of Ca in the mineral, the calcium component of the mineral is transparent to IR [40][41]. However, the phosphate groups interact strongly with IR radiation yielding an elaborate, multi-component absorption band. This is known as ν_3-phosphate peak, well known from bone studies [42].

ATR, transmission and srFTIR KKT infrared spectra:

There are great similarities between spectra obtained by transmission IR from a powder dentine pellet, ATR and the KKT transformed reflectance spectra, as seen in the data shown in Figure 6. For ease of interpretation, the three spectra are normalized to the amide-I peak at 1660 cm^{-1}. It can be seen that, though the measurements are obtained by different IR methods, the ν_2-carbonate, amide I and the shoulder ν_1-phosphate P-O stretching band at 960 cm^{-1} as well as the general intensity patterns, agree between all three methods, and they correspond with results from the literature [22][43][20]. A

comparison of the band assignments between the two most popular methods can be found in Table 1. The peaks do not overlap perfectly, and reveal a shift in some wavenumbers. We tested for a possible difference originating from different spectrometer manufacturers: (i) AIMsight Infrared-Mikroscope (Shimadzu, Japan), (ii) Vertex 70 FTIR (Bruker, Germany) and (iii) Nicolet iN10 (Thermofisher, USA), yet scanning the same samples under similar conditions resulted in identical results (data not shown).

	Band assignment [cm^{-1}]	
Vibration band in dentine	ATR	Transmission
ν_2-carbonate	870 [44] 872[45]	871 [46] 875[30]
ν_3-*phosphate*	1013 [44] 1025[45]	1015 [46] 1020 [30]
Amide I	1650 [44][45]	1650 [46] 1660 [30]

Table 1 – List of the main peaks of dentine and their band assignments by ATR and transmission FTIR methods.

The transmission FTIR peaks of the powdered dentine are generally broader than the peaks obtained by the other methods. This is likely due to multiple scattering enhanced by the small size of the powdered material [47][48]. This is particularly visible for the main phosphate peak, which has a sharper characteristic appearance in both the ATR and srFTIR KKT methods. The transmission spectrum further exhibits a significantly lower relative intensity of the main ν_3-phosphate peak. The ratios between the phosphate and amide-I peak intensities vary from method to method, corresponding to 7.5, 6 and 2.1 for the srFTIR KKT, ATR and transmission FTIR measurements, respectively. This can be explained by the different signal intensities detected by the different methods [49]. The main phosphate peak detected by the ATR method is located at somewhat higher wavenumbers as compared to the srFTIR KKT. The shift of ~ 5 cm^{-1} between the ATR and the srFTIR KKT signal might be due to the known recommendation to correct strong ATR signals to make them comparable to other FTIR methods [11][50]. Under ideal conditions, we would like there to be no band shifts in the peak positions obtained from the KKT srFTIR spectra. However, our application of the Kramer Kronig Transformation is only a numerical approximation in which small uncertainties cannot be avoided [4]. This is in line with previous work that showed that different FTIR methods yield slight differences in band positions[7][26].

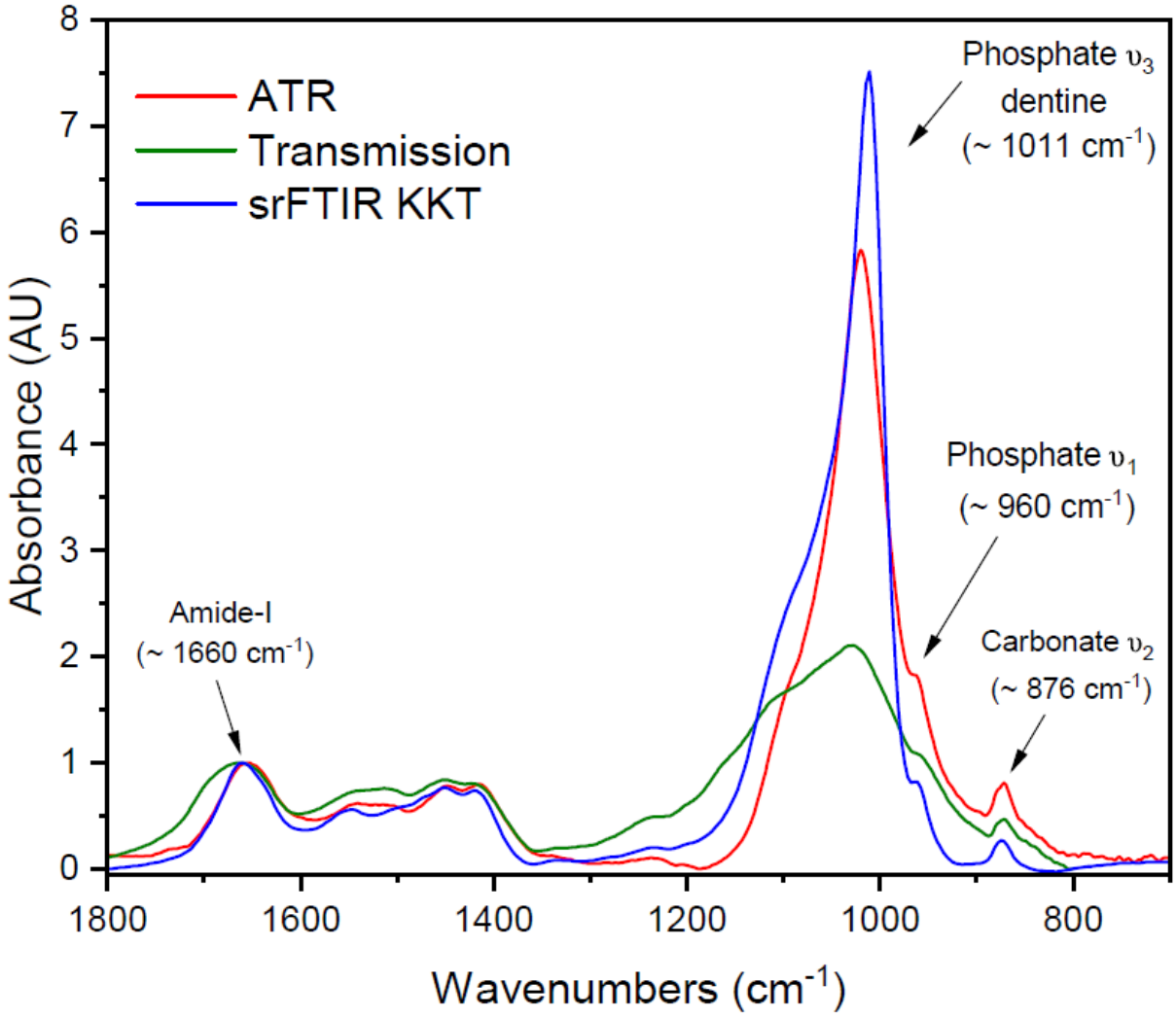

*Figure 6 – Comparison between IR spectra in bovine dentine obtained by the three different, IR methods: ATR (red), Transmission (green) and s*rFTIR KKT *(blue). All curves as normalized to the amide I peak at* 1660 cm^{-1}.

Fitting and unification of the components of the phosphate peak:

For quantitative analysis, the KKT transformed spectra of both dentine and enamel were curve-fitted between 960 and 1200 cm^{-1} and deconvoluted using an in-house Python code. Based on the work of Magne [30], five different gaussian curves were used to deconvolve the components of the ν_3-phosphate peak, fixed at 1015, 1037, 1050, 1090, and 1148 cm^{-1} as listed in Table 2. Thus, the deconvolution of the ν_3-phosphate peak made use of Gaussian functions with peaks centers summarized in Table 1, corresponding to $\nu_3 - PO_4^{3-}$ reported for poorly crystalline apatite, $\nu_3 - PO_4^{3-}$ reported for stoichiometric apatite, HPO_4^{2-} reported for apatite with B-Type carbonate substitution, PO_4^{3-} in stoichiometric apatite and 1148 cm^{-1} for acid phosphate, $\nu_1 - PO_4^{3-}$. The fitting results (Fig. 7) showed negligible differences whether the wavelength centers were fixed to the proposed positions or when they were allowed to shift within a range of ±10 cm^{-1}.

Wavenumber	Band assignment	
1015 cm^{-1}	$\nu_3 - PO_4^{3-}$	as observed in poorly crystalline apatite
1037 cm^{-1}	$\nu_3 - PO_4^{3-}$	as reported for stoichiometric apatite
1050 cm^{-1}	HPO_4^{2-}	containing apatite and Type B carbonate apatite
1090 cm^{-1}	$\nu_3 - PO_4^{3-}$	in stoichiometric apatite
1148 cm^{-1}	HPO_4^{2-}	acid phosphate

Table 2 – List of the peak assignments used to deconvolute the phosphate peak between 960 and 1200 cm^{-1}.

Example srFTIR KKT spectra of enamel and dentine along with the peaks used for fitting are shown in Figure 7. The resulting fit of all peaks agrees well with the original spectrum in both cases. The dentine fit reached 0.99 and the one for enamel 0.97 as chi-square value [51], demonstrating a reliable result.

In dentine, the 1015 cm^{-1} vibration dominates the shape of the ν_3-phosphate peak, with no identifiable acid phosphate contribution, as indicated by the absence of the 1148 cm^{-1} band. In contrast, the enamel spectrum shows a slightly reduced intensity for the 1050 cm^{-1} band, a less prominent role for the 1015 cm^{-1} vibration and an increased contribution of the 1037 cm^{-1} vibration, amounting to 0.75 the intensity of the 1015 cm^{-1} peak The 1148 cm^{-1} band, corresponding to acid phosphate, appears only in the enamel spectra, as previously reported [52].

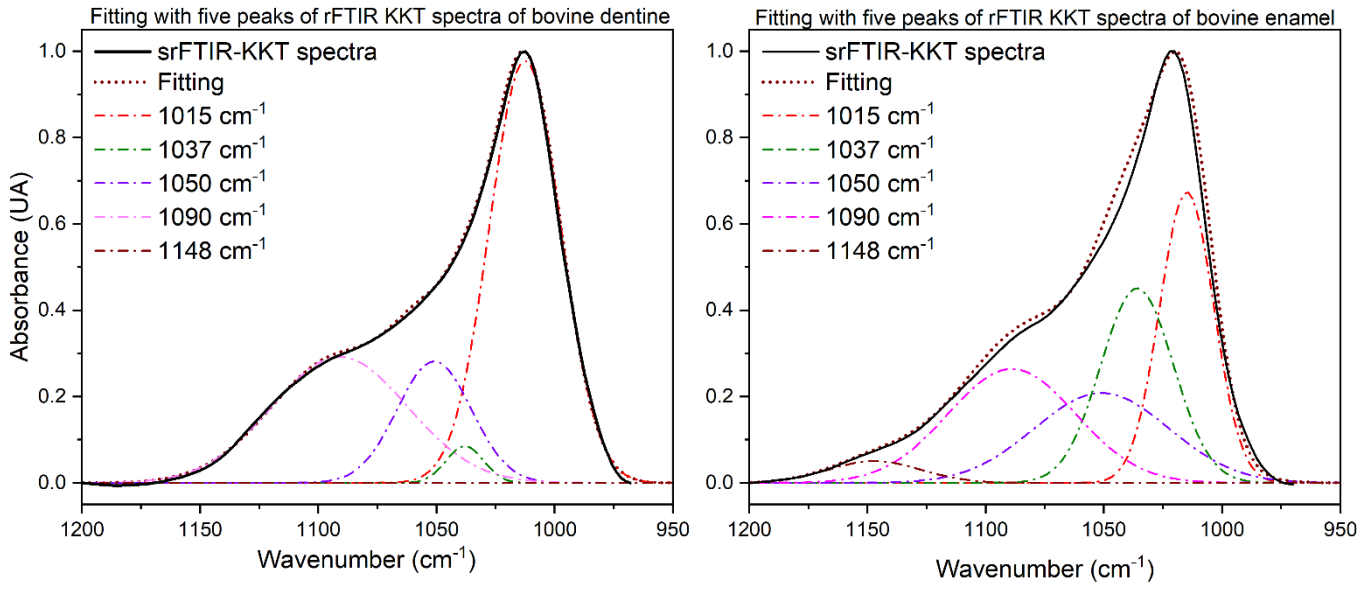

Figure 7 – Example spectra and fit results for the ν_3-phosphate peak identified in all measurements between 960 and 1200 cm^1. The five main Gaussian peaks correspond to well documented phosphate ν_3- and HPO_4^{2-} vibrations. The Gaussian curves are plotted in colors as listed in the legend; the combined fits are shown with a brown dashed line ("Fitting"). For both enamel and dentine, the fitting follows closely the srFTIR KKT, with chi square values of 0.99 and 0.97 of spectra indicative of a reliable fit. The fit for dentine does not require the 1148 cm^{-1} contribution, suggestive of a total lack of significant amounts of acid phosphate in dentine.

Integration maps of the fitted phosphate peaks

All intensities, plotted on X-Y coordinates were converted into 2D maps produced using Fiji [53] to show the distribution of the values across the surfaces of the scanned A, B, C & D teeth.

By plotting the intensities of the fitted peaks, we obtain srFTIR KKT maps of the presumed chemical components measured across entire tooth sections in a non-contact manner. These can be related to our complementary measurements to elucidate the extent to which the spectra reveal the microstructure or the chemical composition of the different, regionally-varying tooth components. In each map, brighter colors indicate a stronger IR interaction, though it is not clear if the interaction is due to only chemical absorption or due to some other scattering and hence loss of signal, appearing as IR "absorption".

The maps are grouped into peaks corresponding to stretches of the ν_3-phosphate vibrations at 1015 cm^{-1}, 1037 cm^{-1} and 1090 cm^{-1} while complementary maps depict the stretches of acid phosphate containing apatite (1050 cm^{-1} , HPO_4^{2-}) and Type B carbonate apatite (1148 cm^{-1}, $\nu_1 HPO_4^{2-}$).

Figure 8 compares maps of the 4 teeth presented in Figures 1 and 2. Intriguingly, despite some variations in intensity, the overall distribution of srFTIR KKT intensities between enamel on the outside and dentine surrounding the pulp are quite similar revealing highly comparable trends. This suggests that either there is a minimal chemical difference between different young bovine teeth (and the human tooth), or that the conserved microstructures (elongated crystals in enamel, tubules and variable mineral densities in dentine) have a much stronger effect on the srFTIR signal. Both suggest that bovine teeth are indeed decent substitutes for intact young human teeth, when required in research [54]. Indeed, bovine teeth are often used in research to supplement human teeth, reducing the large variability in tooth exposure and use in different humans, including environmental, genetic and dental treatment histories [55].

Since there are known differences in microstructure across teeth, our analysis and comparisons with complementary optical images and mapping by SEM and μXRF paves the way to assess the possible roles of microstructure scattering and texture on the srFTIR signal. To do so, we make use of the well-known regionally varying signatures of both the mineral and organics, especially in the young non-treated and very self-similar bovine teeth. Since all enamel is highly crystalline and of approximately the same chemical composition as the mineral in dentine, in each tooth, enamel serves as a comparable reference (lacking collagen and hence lacking amide I fingerprints). Specifically, enamel and dentine differ in the mineral density and nanocrystal size and packing, though in both cases the mineral is carbonated apatite. Similar to bone, dentine contain less mineral (70%) and more organic material while enamel comprises prisms of co-aligned elongated crystals (95%) [56]. The peak at 1037 cm^{-1} always shows the brightest color in the region where the outer enamel ring is located. This suggests that the srFTIR KKT signal is proportional to the density of the chemical vibration of "stoichiometric apatite", and is thus expected to be brighter in the regions of high density apatite [57]. Other vibrations within the ν_3-phosphate peak do not show this trend, suggestive of a strong chemical signature component of this peak. Curiously, the absorption band at 1148 cm^{-1} is a good indicator for enamel, appearing exclusively to that tissue, though associated with the chemical groups of acid phosphate. We noted that the intensity of this peak is not dependent on the orientation of the measurement with respect to cross sectional or longitudinal slices in teeth, such that it is likely that role that scattering plays a less pronounced than chemical absorption. This raises the possibility that far more acid phosphate is indeed present in enamel e.g. between or on the outer margins of the long crystals, a signature that we did not identify in dentine.

Comparisons between certain chemical signatures with the optical images of Figure 1 reveal "stripes" that are clearly identifiable in samples A and C (marked by white rectangle). These appear in the FTIR images of the same samples as "stains" observed in the 1015 cm^{-1} and 1050 cm^{-1} vibrations. The optical image color difference suggests a difference in light scattering which may be due to different density and mineralization of the tubules. On the other hand, there may be smaller crystals in those regions. Further work with other methods may be needed to better understand this observation.

When focusing only on dentine, the 1090 cm^{-1} band (Figure 8) of the srFTIR KKT IR map resembles the XRF phosphorus maps in Figure 3: images of the same teeth show similar distribution of features, albeit at very different resolutions due to limitations of our rather low-spatial-resolution srFTIR mapping of the large samples. Some studies explain the dependence between the light propagation in human dentine and its microstructure [58], as well as how the crystallite size and structural carbonate content in bone shapes the infrared peaks [59]. This might suggest that for this peak, srFTIR chemical features strongly mix with light scattering appearing as absorption due to the tubule microstructure.

Integration maps of Carbonate and Amide I

The areas under the bands of amide I (1,660 cm^{-1}) and ν_2-carbonate (875 cm^{-1}) peaks were integrated simply by removing a baseline joining the extreme points of each peak, and they are plotted as 2D maps produced using Fiji showing the distribution of the intensities across the scanned A, B, C and D teeth.

Maps of the peaks corresponding to the ν_2-carbonate (850-900 cm^{-1}) and the amide I (1592-1720 cm^{-1}) peaks, shown in Figure 9, reveal a relatively homogeneous distribution of carbonate. The ν_2-carbonate is distributed rather uniformly in the central ring of the dentine and shows a higher content than in enamel. Near the pulp chamber and near the border between dentine and enamel the carbonate content is reduced. In enamel, it can be seen that there are higher levels in the inner enamel as compared with in the outer. A similar observation was previously reported by Xu using Raman spectroscopy. [60].

A stronger signal of the amide I is observed in the outer part of the dentine, near the DEJ, and to some extent also in the rim around the pulp chamber. In these regions there is a higher organic concentration and lower mineral density, which well matches these results. There is no presence of amide I in the enamel as this tissue does not contain collagen [61], therefore, the srFTIR KKT data is well suited to map collagen density variations across tooth samples.

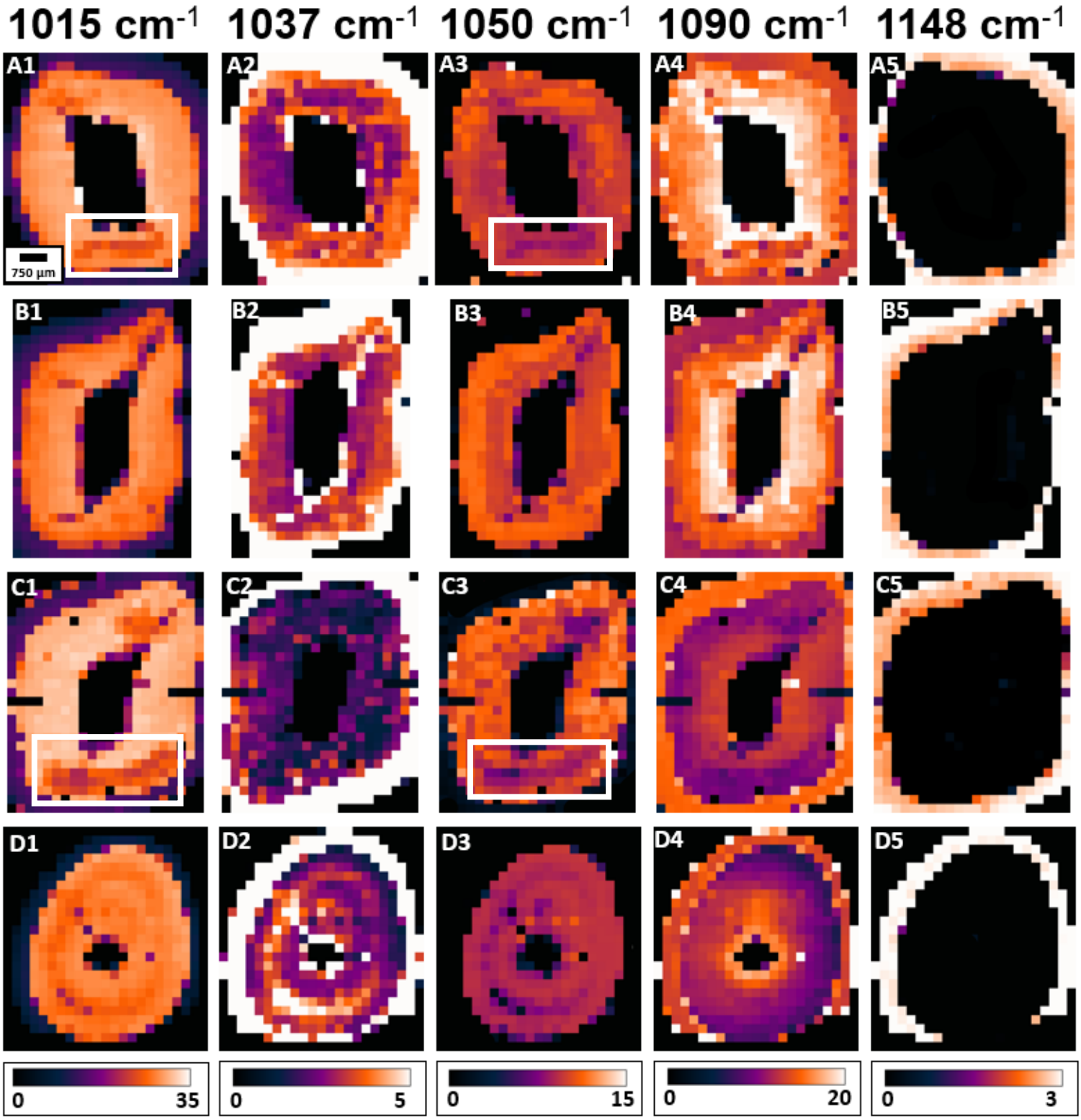

Figure 8 – Maps of three bovine teeth (A, B and C) and one human tooth (D) showing results of the integration of each Gaussian curve used to deconvolute the main phosphate peak in the range of 960 to 1200 cm^{-1}. The scale bar in map A1 is valid for all the maps. The calibration bar beneath each column is given in integrated absorption values, always following the premise that brighter colors indicate higher intensities. A white rectangle in sample A1-A3 and in C1-C3 show the same "stains" already identified with a purple rectangle in the optical images in Figure 1.

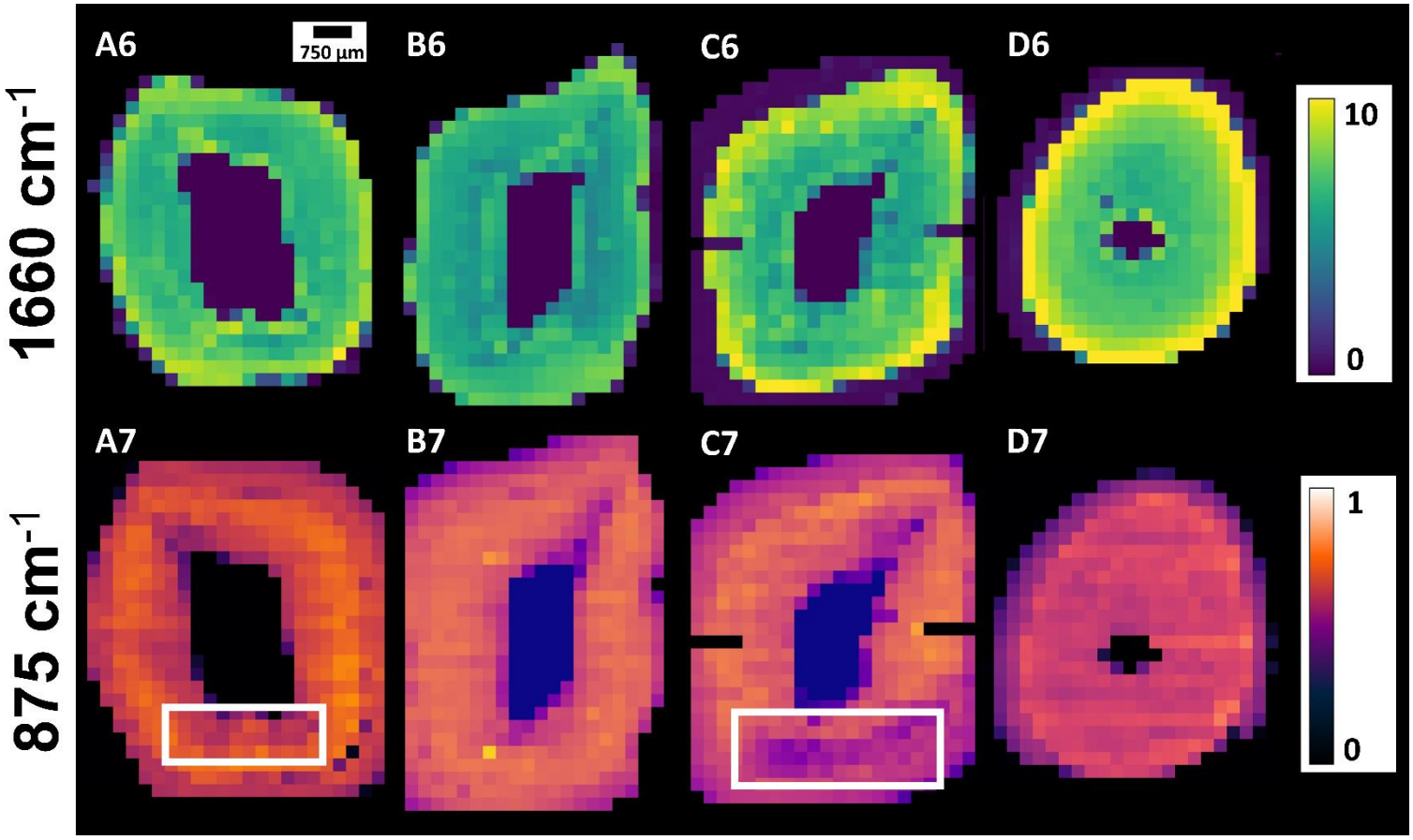

Figure 9 – Maps of three bovine teeth (A, B and C) and one human teeth (D) showing the integration of the amide I peak (1660 cm^{-1}) on the top row and ν_2-carbonate peak (875 cm^{-1}) in the bottom row. The scalebar seen in image A6 is valid for all maps. On the right, the calibration bars are the same for all maps in each row. The amide I intensity is higher near the DEJ (see Fig. 1) and more-or-less uniform besides some traces of brighter signal surrounding the pulp rim. In these regions the mineral density is lower thus a higher signal of collagen is detected. There is no presence of amide I in the enamel. The ν_2-carbonate signal is stronger in dentine than in enamel. The signal is rather weak and fairly uniform, as is expected for a low% carbonate content of dentine ([55]*). A "stain" already mentioned and visible in the optic image and in the 1015 cm^{-1} and in the 1050 cm^{-1} vibrations also appears in the carbonate map of A7, very slightly, and in C7.*

Spatial covariance correlation analysis

To understand how the different components of the phosphate peak vary in space and in relation to the organics, we determined the similarity in local map patterns in all of the srFTIR KKT data using similarity of patterns (SIP) comparisons. These provide positive or negative correlation estimates between the compared maps. Figure 10 shows the results for two comparisons: a) amide I versus the 1015 cm^{-1} absorption signal and b) amide I versus the 1037 cm^{-1} absorption signal. The SIP metric quantified the degree to which the patterns of intensity distributions are correlated and how they vary across the sample surface. A SIP value approaching 1, indicates that the compared maps (e.g. amide I versus the 1015 cm^{-1} absorption band) vary in space in a similar manner. When the SIP correlation is negative, the intensity distributions are anti-correlated, such that patterns of high intensity in one map correlate with patterns of low intensity in the other.

The comparisons shown in Figure 10 reveal a high correlation between high intensities of the amide I and the 1015 cm^{-1} absorption peak across dentine. We conclude that these IR signals arise from the mineralized collagen fibrils (collagen and mineral) regardless of different textures, and therefore they likely represent the chemistry of the composite in dentine. The second comparison between amide I and the 1037 cm^{-1} map shows a high positive correlation near the pulp but an inverse SIP correlation near the DEJ. This indicates that in some regions, there is an inverse relationship between the peaks, in particularly inversed in the so called "soft dentine" zone situated between enamel and the main dentine bulk [36]. This suggests that, unlike the 1015 cm^{-1} peak, the 1037 cm^{-1} absorption peak is strongly affected by changes in the microstructure texture suggesting that is is strongly affected by scattering rather than chemical absorption in dentine samples. We therefore conclude that the deconvolution helps to isolate peaks relating to the chemistry, from peaks that are mainly affected by scattering, thus not recommended for chemical comparisons.

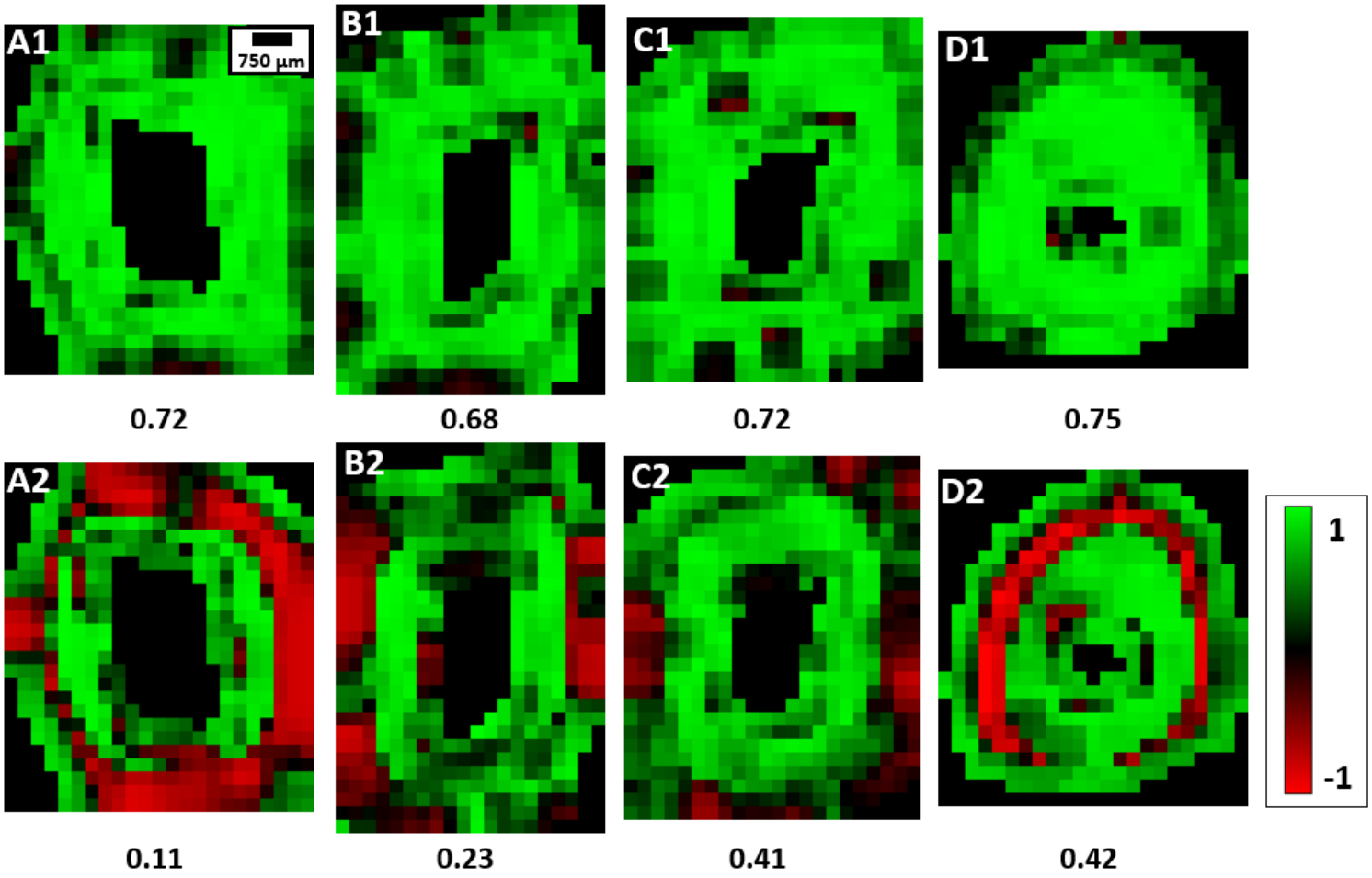

Figure 10 – SIP (similarity in patterns) maps of the correlation between amide I and the 1015 cm^{-1} absorption band (top row) and amide I and the 1037 cm^{-1} absorption band (bottom row). The scale bar in sample A1 is valid for all maps. The calibration bar on the right side indicates a highly correlated area in green and an inversed correlated area in red. amide I compared with the 1015 cm^{-1} band has a consistent correlation across the sample, while for the amide I and the 1037 cm^{-1} absorption band show a positive correlation near the pulp and an inverse correlation near in the outer regions of dentine near the DEJ.

Conclusion

The objective of this study was to investigate the potential of Fourier Transform Infrared Spectroscopy (FTIR) in reflection mode for mapping the distribution of chemical groups across entire tooth cross-sections, in particular, to be able to identify non-destructively, variations in chemistry across entire tooth sections spaning many mm in diameter. This approach makes it possible to maintain spatial information about the tooth structures and to avoid any contact during high-chemical sensitivity FTIR measurements, specifically avoiding ATR that requires applying forces that could alter the state of stress within the samples. To achieve optimal reflection signals, the samples must be meticulously polished to a mirror finish and must be complete dehydrated to reveal the subtle gradients in microstructure and chemistry, while reducing the influence of water on the IR spectroscopy results.

The acquired reflectance spectra were processed using an in-house implementation of the Kramers-Kronig transformation, provided in the supplementary information section and available on GitHUB [27].

The transformed reflection spectra demonstrated high comparability with spectral features that are commonly obtained from measurements by Attenuated Total Reflection (ATR), the more widely used FTIR method. The srFTIR features are also highly compatible with measurements obtained by transmission mode FTIR, typically performed on powdered samples devoid of spatial mapping information. Minor differences in band positions were observed and may be attributed to variations in spectral resolution and post-processing corrections, known to be necessity for spectral correction in ATR, as recommended by spectrometer manufacturers [62].

Our results provide insights into how the vibrations of the ν_3-phosphate peaks vary across the tooth surface, allowing a clear identification of gradients and local differences in chemistry but also in tissue texture (in both the enamel layer in the outer ring and dentine) with variable morphologies of dentinal tubules that are visible across the samples. Comparisons with optical images showed that to some extent, the microstructure influences the absorption intensity due to scatter of the IR spectra. This brings to focus that FTIR is not only sensitive to chemical groups but is also affected by light scattering in the tooth microstructures. These findings could aid for example, in understanding gradients in chemical or microstructural changes across samples (e.g. ageing and development of sclerotic dentine).

Our maps of intensity variations in the ν_2-carbonate and amide-I absorption peaks revealed the spatial distribution of these chemical groups. Such maps, combined with analysis of the spatial variation and correlation of the SIP index, may offer valuable insights into understanding the spatial changes in the microstructure or chemistry of dentine, with possible implication to changes due to degradation.

In agreement with the already reported studies , our results indicate a that bovine teeth are a good approximation for human teeth given the fact that the general patterns and tendencies regarding chemistry and infrared spectra are similar [54][55].

Data Availability:

The raw data used for this manuscript including all specular reflectance maps and µXRF of all teeth can be found and wonloaded from: https://doi.org/10.7910/DVN/R7CKUA.

Author contributions:

Conceptualization: FL and PZ. Resources: LP, PL, IM, PZ. Investigation: FL, PL, OM. Formal analysis and visualization: FL and OM. Python coding: OL and FL Writing – review and editing: FL, HE, OM, LP, PL, IM, PZ. Supervision: PZ. Funding acquisition: IM and PZ.

Acknowledgments:

FL and PZ thank the DFG (Deutsche Forschungsgemeinschaft) via FOR2804 (InterDent) TPZ and TP1 through grants awarded to PZ and IM. We are thankful to Prof. Birgit Kanngießer for the access to the µXRF instrumentation in TU-Berlin, to BESSY II (Helmholtz-Zentrum Berlin) for the access to the FTIR laboratory microscope and to Ms. Pilar Fernández Paradela (Charité Universitätsmedizin) for her support in FTIR measurements.

Ethical approval

This article does not contain any studies with human participants or animals performed by any of the authors.

Compliance with ethical standards

P.L. is the author of CytoSpec, a software package for vibrational hyperspectral imaging. The other authors declare no competing financial interests.

References

[1] A. Nanci, *Ten cate's oral histology*, 10th ed. Professor, Faculty of Dentistry, University of Montreal, Montreal, Quebec, Canada: Elsevier - Health Sciences Division, 2024.

[2] G. W. Marshall, "T HE M ECHANICAL P ROPERTIES OF H UMAN D ENTIN : A C RITICAL R EVIEW AND R E - EVALUATION OF THE D ENTAL L ITERATURE," pp. 13–29, 1980.

[3] L. Angker and M. V. Swain, "Nanoindentation: Application to dental hard tissue investigations," *J. Mater. Res.*, vol. 21, no. 8, pp. 1893–1905, Aug. 2006, doi: 10.1557/jmr.2006.0257.

[4] J. Kolmas *et al.*, "Incorporation of carbonate and magnesium ions into synthetic hydroxyapatite: The effect on physicochemical properties," *J. Mol. Struct.*, vol. 987, no. 1–3, pp. 40–50, 2011, doi: 10.1016/j.molstruc.2010.11.058.

[5] C. de C. A. Lopes, P. H. J. O. Limirio, V. R. Novais, and P. Dechichi, "Fourier transform infrared spectroscopy (FTIR) application chemical characterization of enamel, dentin and bone," *Appl. Spectrosc. Rev.*, vol. 53, no. 9, pp. 747–769, 2018, doi: 10.1080/05704928.2018.1431923.

[6] M. J. Baker *et al.*, "Using Fourier transform IR spectroscopy to analyze biological materials," *Nat. Protoc.*, vol. 9, no. 8, pp. 1771–1791, 2014, doi: 10.1038/nprot.2014.110.

[7] A. Boskey and N. Pleshko Camacho, "FT-IR imaging of native and tissue-engineered bone and cartilage," *Biomaterials*, vol. 28, no. 15, pp. 2465–2478, 2007, doi: 10.1016/j.biomaterials.2006.11.043.

[8] T. A. Surovell and M. C. Stiner, "Standardizing infra-red measures of bone mineral crystallinity: An experimental approach," *J. Archaeol. Sci.*, vol. 28, no. 6, pp. 633–642, 2001, doi: 10.1006/jasc.2000.0633.

[9] Y. Chen, C. Zou, M. Mastalerz, S. Hu, C. Gasaway, and X. Tao, "Applications of micro-fourier transform infrared spectroscopy (FTIR) in the geological sciences—A Review," *Int. J. Mol. Sci.*, vol. 16, no. 12, pp. 30223–30250, 2015, doi: 10.3390/ijms161226227.

[10] M. Boulet-Audet, T. Buffeteau, S. Boudreault, N. Daugey, and M. Pézolet, "Quantitative determination of band distortions in diamond attenuated total reflectance infrared spectra," *J. Phys. Chem. B*, vol. 114, no. 24, pp. 8255–8261, 2010, doi: 10.1021/jp101763y.

[11] J. Aufort, L. Ségalen, C. Gervais, C. Brouder, and E. Balan, "Modeling the attenuated total reflectance infrared (ATR-FTIR) spectrum of apatite," *Phys. Chem. Miner.*, vol. 43, no. 9, pp. 615–626, 2016, doi: 10.1007/s00269-016-0821-x.

[12] F. Friedrich and P. G. Weidler, "Contact pressure effects on vibrational bands of kaolinite during infrared spectroscopic measurements in a diamond attenuated total reflection cell," *Appl. Spectrosc.*, vol. 64, no. 5, pp. 500–506, 2010, doi: 10.1366/000370210791211619.

[13] K. Sauer, I. Zizak, J. B. Forien, A. Rack, E. Scoppola, and P. Zaslansky, "Primary radiation damage in bone evolves via collagen destruction by photoelectrons and secondary emission self-absorption," *Nat. Commun.*, vol. 13, no. 1, pp. 1–12, 2022, doi: 10.1038/s41467-022-34247-z.

[14] J. B. Forien *et al.*, "Compressive Residual Strains in Mineral Nanoparticles as a Possible Origin of Enhanced Crack Resistance in Human Tooth Dentin," *Nano Lett.*, vol. 15, no. 6, pp. 3729–3734, 2015, doi: 10.1021/acs.nanolett.5b00143.

[15] J. B. Forien *et al.*, "Water-Mediated Collagen and Mineral Nanoparticle Interactions Guide Functional Deformation of Human Tooth Dentin," *Chem. Mater.*, vol. 28, no. 10, pp. 3416–3427, 2016, doi: 10.1021/acs.chemmater.6b00811.

[16] V. Lucarini, J. J. Saarinen, K.-E. Peiponen, and E. M. Vartiainen, *Kramers-kronig relations in optical materials research*, 2005th ed. Berlin, Germany: Springer, 2005. doi: 10.1007/b138913.

[17] D. M. Roessler, "Kramers-Kronig analysis of reflection data," *Br. J. Appl. Phys.*, vol. 16, no. 8, pp. 1119–1123, 1965, doi: 10.1088/0508-3443/16/8/310.

[18] A. B. Kuzmenko, "Kramers–Kronig constrained variational analysis of optical spectra," *Rev. Sci. Instrum.*, vol. 76, no. 8, Aug. 2005, doi: 10.1063/1.1979470.

[19] I. H. Kim, J. S. Son, B. K. Min, Y. K. Kim, K. H. Kim, and T. Y. Kwon, "A simple, sensitive and non-destructive technique for characterizing bovine dental enamel erosion: Attenuated total reflection Fourier transform infrared spectroscopy," *Int. J. Oral Sci.*, vol. 8, no. December 2015, pp. 54–60, 2016, doi: 10.1038/ijos.2015.58.

[20] P. Seredin *et al.*, "A Study of the Peculiarities of the Formation of a Hybrid Interface Based on Polydopamine between Dental Tissues and Dental Composites, Using IR and Raman Microspectroscopy, at the Submicron Level," *Int. J. Mol. Sci.*, vol. 24, no. 14, 2023, doi: 10.3390/ijms241411636.

[21] P. Seredin, D. Goloshchapov, Y. Ippolitov, and J. Vongsvivut, “Development of a new approach to diagnosis of the early fluorosis forms by means of FTIR and Raman microspectroscopy,” *Sci. Rep.*, vol. 10, no. 1, pp. 1–12, 2020, doi: 10.1038/s41598-020-78078-8.

[22] S. Diez-García, M. J. Sánchez-Martín, J. M. Amigo, and M. Valiente, “Combination of Two Synchrotron Radiation-Based Techniques and Chemometrics to Study an Enhanced Natural Remineralization of Enamel,” *Anal. Chem.*, vol. 94, no. 13, pp. 5359–5366, 2022, doi: 10.1021/acs.analchem.1c05498.

[23] C. Babot-Marquillas *et al.*, “Tooth whitening effects on dental enamel, oxidation or reduction? Comparison of physicochemical alterations in bovine enamel using Synchrotron-based Micro-FTIR,” *Dent. Mater.*, vol. 38, no. 4, pp. 670–679, 2022, doi: 10.1016/j.dental.2022.02.006.

[24] W. Tesch, N. Eidelman, P. Roschger, F. Goldenberg, K. Klaushofer, and P. Fratzl, “Graded microstructure and mechanical properties of human crown dentin,” *Calcif. Tissue Int.*, vol. 69, no. 3, pp. 147–157, 2001, doi: 10.1007/s00223-001-2012-z.

[25] F. Förste *et al.*, “Quantification routines for full 3D elemental distributions of homogeneous and layered samples obtained with laboratory confocal micro XRF spectrometers,” *J. Anal. At. Spectrom.*, vol. 37, no. 8, pp. 1687–1695, 2022, doi: 10.1039/d2ja00119e.

[26] P. Lichvár, M. Liška, and D. Galusek, “What is the true Kramers-Kronig transform?,” *Ceram. - Silikaty*, vol. 46, no. 1, pp. 25–27, 2002.

[27] L. F. Lenz Ole, “FTIR-Kramers-Kronig-Lizzi-Lenz.” [Online]. Available: https://github.com/olelenz/FTIR-Kramers-Kronig-Lizzi-Lenz

[28] “CytoSpec 2.10.01.” [Online]. Available: www.cytospec.com

[29] E. L. Jones, L. Rendell, E. Pirotta, and J. A. Long, “Novel application of a quantitative spatial comparison tool to species distribution data,” *Ecol. Indic.*, vol. 70, pp. 67–76, 2016, doi: 10.1016/j.ecolind.2016.05.051.

[30] D. Magne, P. Weiss, J. M. Bouler, O. Laboux, and G. Daculsi, “Study of the maturation of the organic (type I collagen) and mineral (nonstoichiometric apatite) constituents of a calcified tissue (dentin) as a function of location: A fourier transform infrared microspectroscopic investigation,” *J. Bone Miner. Res.*, vol. 16, no. 4, pp. 750–757, 2001, doi: 10.1359/jbmr.2001.16.4.750.

[31] M. E. Fleet, “Infrared spectra of carbonate apatites: v2-Region bands,” *Biomaterials*, vol. 30, no. 8, pp. 1473–1481, 2009, doi: 10.1016/j.biomaterials.2008.12.007.

[32] Z. Wang, A. C. Bovik, H. R. Sheikh, and E. P. Simoncelli, “Image quality assessment: From error visibility to structural similarity,” *IEEE Trans. Image Process.*, vol. 13, no. 4, pp. 600–612, 2004, doi: 10.1109/TIP.2003.819861.

[33] S. Weiner *et al.*, “Peritubular dentin formation: Crystal organization and the macromolecular constituents in human teeth,” *J. Struct. Biol.*, vol. 126, no. 1, pp. 27–41, 1999, doi: 10.1006/jsbi.1999.4096.

[34] R. Garberoglio and M. Brännström, “Scanning electron microscopic investigation of human dentinal tubules,” *Arch. Oral Biol.*, vol. 21, no. 6, pp. 355–362, 1976, doi: 10.1016/S0003-9969(76)80003-9.

[35] I. A. Mjör, “Human coronal dentine: Structure and reactions,” *Oral Surgery, Oral Med. Oral Pathol.*, vol. 33, no. 5, pp. 810–823, 1972, doi: 10.1016/0030-4220(72)90451-3.

[36] P. Zaslansky, A. A. Friesem, and S. Weiner, “Structure and mechanical properties of the soft zone separating bulk dentin and enamel in crowns of human teeth: Insight into tooth function,” *J. Struct. Biol.*, vol. 153, no. 2, pp. 188–199, Feb. 2006, doi: 10.1016/j.jsb.2005.10.010.

[37] R. Z. LeGeros, “Properties of Osteoconductive Biomaterials: Calcium Phosphates,” *Clin. Orthop. Relat. Res.*, vol. 395, pp. 81–98, Feb. 2002, doi: 10.1097/00003086-200202000-00009.

[38] A. E. W. Miles, *Structural and chemical organization of teeth: V. 1*. San Diego, CA: Academic Press, 1967.

[39] Y. A. Lazarev, B. A. Grishkovsky, and T. B. Khromova, “Amide I band of IR spectrum and structure of collagen and related polypeptides,” *Biopolymers*, vol. 24, no. 8, pp. 1449–1478, 1985, doi: 10.1002/bip.360240804.

[40] A. Ślósarczyk, Z. Paszkiewicz, and C. Paluszkiewicz, “FTIR and XRD evaluation of carbonated hydroxyapatite powders synthesized by wet methods,” *J. Mol. Struct.*, vol. 744–747, no. SPEC. ISS., pp. 657–661, 2005, doi: 10.1016/j.molstruc.2004.11.078.

[41] I. Rehman and W. Bonfield, “Characterization of hydroxyapatite and carbonated apatite by photo acoustic FTIR spectroscopy,” *J. Mater. Sci. Mater. Med.*, vol. 8, no. 1, pp. 1–4, 1997, doi: 10.1023/A:1018570213546.

[42] E. A. Taylor and E. Donnelly, “Raman and Fourier transform infrared imaging for characterization of bone material properties,” *Bone*, vol. 139, p. 115490, 2020, doi: 10.1016/j.bone.2020.115490.

[43] E. P. Paschalis, S. Gamsjaeger, and K. Klaushofer, “Vibrational spectroscopic techniques to assess bone quality,”

Osteoporos. Int., vol. 28, no. 8, pp. 2275–2291, 2017, doi: 10.1007/s00198-017-4019-y.

[44] Y. Liu, X. Yao, Y. W. Liu, and Y. Wang, "A Fourier Transform Infrared Spectroscopy Analysis of Carious Dentin from Transparent Zone to Normal Zone," *Caries Res.*, vol. 48, no. 4, pp. 320–329, 2014, doi: 10.1159/000356868.

[45] G. H. Yassen, T.-M. G. Chu, G. Eckert, and J. A. Platt, "Effect of Medicaments Used in Endodontic Regeneration Technique on the Chemical Structure of Human Immature Radicular Dentin: An In Vitro Study," *J. Endod.*, vol. 39, no. 2, pp. 269–273, Feb. 2013, doi: 10.1016/j.joen.2012.09.020.

[46] S. Bohic, D. Heymann, J. A. Pouëzat, O. Gauthier, and G. Daculsi, "Transmission FT-IR microspectroscopy of mineral phases in calcified tissues," *Comptes Rendus l'Académie des Sci. - Ser. III - Sci. la Vie*, vol. 321, no. 10, pp. 865–876, 1998, doi: 10.1016/s0764-4469(99)80027-4.

[47] J. M. Thompson, *Infrared Spectroscopy*. Jenny Stanford Publishing, 2018. doi: 10.1201/9781351206037.

[48] E. Balan *et al.*, "Line-broadening effects in the powder infrared spectrum of apatite," *Phys. Chem. Miner.*, vol. 38, no. 2, pp. 111–122, 2011, doi: 10.1007/s00269-010-0388-x.

[49] Z. M. Khoshhesab, "Reflectance IR Spectroscopy," in *Infrared Spectroscopy - Materials Science, Engineering and Technology*, InTech, 2012. doi: 10.5772/37180.

[50] "Mayerhöfer et al. - 2020 - The Bouguer-Beer-Lambert Law Shining Light on the.pdf."

[51] I. Wendt and C. Carl, "The statistical distribution of the mean squared weighted deviation," *Chem. Geol. Isot. Geosci. Sect.*, vol. 86, no. 4, pp. 275–285, Apr. 1991, doi: 10.1016/0168-9622(91)90010-T.

[52] J. Arends and C. L. Davidson, "HPO(Formula presented.) Content in enamel and artificial carious lesions," *Calcif. Tissue Res.*, vol. 18, no. 1, pp. 65–79, 1975, doi: 10.1007/BF02546227.

[53] J. Schindelin *et al.*, "Fiji: An open-source platform for biological-image analysis," *Nat. Methods*, vol. 9, no. 7, pp. 676–682, 2012, doi: 10.1038/nmeth.2019.

[54] G. H. Yassen, J. A. Platt, and A. T. Hara, "Bovine teeth as substitute for human teeth in dental research: a review of literature.," *J. Oral Sci.*, vol. 53, no. 3, pp. 273–282, 2011, doi: 10.2334/josnusd.53.273.

[55] J. De Dios Teruel, A. Alcolea, A. Hernández, and A. J. O. Ruiz, "Comparison of chemical composition of enamel and dentine in human, bovine, porcine and ovine teeth," *Arch. Oral Biol.*, vol. 60, no. 5, pp. 768–775, 2015, doi: 10.1016/j.archoralbio.2015.01.014.

[56] M. A. H. De Menezes Oliveira *et al.*, "Microstructure and mineral composition of dental enamel of permanent and deciduous teeth," *Microsc. Res. Tech.*, vol. 73, no. 5, pp. 572–577, May 2010, doi: 10.1002/jemt.20796.

[57] K. Sarna-Boś, K. Skic, P. Boguta, A. Adamczuk, M. Vodanovic, and R. Chałas, "Elemental mapping of human teeth enamel, dentine and cementum in view of their microstructure," *Micron*, vol. 172, no. May, 2023, doi: 10.1016/j.micron.2023.103485.

[58] A. Kienle, F. K. Forster, R. Diebolder, and R. Hibst, "Light propagation in dentin: influence of microstructure on anisotropy," *Phys. Med. Biol.*, vol. 48, no. 2, pp. N7–N14, Jan. 2003, doi: 10.1088/0031-9155/48/2/401.

[59] G. Dal Sasso, Y. Asscher, I. Angelini, L. Nodari, and G. Artioli, "A universal curve of apatite crystallinity for the assessment of bone integrity and preservation," *Sci. Rep.*, vol. 8, no. 1, pp. 1–13, 2018, doi: 10.1038/s41598-018-30642-z.

[60] C. Xu, R. Reed, J. P. Gorski, Y. Wang, and M. P. Walker, "The distribution of carbonate in enamel and its correlation with structure and mechanical properties," *J. Mater. Sci.*, vol. 47, no. 23, pp. 8035–8043, Dec. 2012, doi: 10.1007/s10853-012-6693-7.

[61] R. S. Lacruz, S. Habelitz, J. T. Wright, and M. L. Paine, "Dental Enamel Formation and Implications for Oral Health and Disease," *Physiol. Rev.*, vol. 97, no. 3, pp. 939–993, Jul. 2017, doi: 10.1152/physrev.00030.2016.

[62] J. Grdadolnik, "Acta Chim. Slov. 2002 , 49 , 631 − 642.," *Acta Chim.Slov*, vol. 49, pp. 631–642, 2002.